International Journal of Solids and Structures 49 (2012) 2668–2680

Contents lists available at SciVerse ScienceDirect

International Journal of Solids and Structures

journal homepage: www.elsevier.com/locate/ijsolstr

Quasi-soft opto-mechanical behavior of photochromic liquid crystal elastomer: Linearized stress–strain relations and finite element simulations

Yin Lin, Lihua Jin [1], Yongzhong Huo *

Department of Mechanics and Engineering Science, Fudan University, Shanghai 200433, China

ARTICLE INFO

Article history:
Received 4 January 2012
Received in revised form 24 May 2012
Available online 7 June 2012

Keywords:
Liquid crystal elastomer
Light-induced bending
Opto-mechanical effect
Soft elasticity
Finite element simulation

ABSTRACT

Based on the neo-classical elastic energy of liquid crystal elastomers, the opto-mechanical behavior is modeled by considering the effect of photoisomerization on the nematic-isotropic transition of liquid crystal phase. Linearized stress–strain relation is derived for infinitesimal deformations with a very unusual shear stress that does not vanish identically as in the case of the soft behavior but is proportional to the rotation of directors. In other words, the shear stress depends on both the shear strain and the skew symmetric part of the displacement gradient with the shear modulus induced by the effect of photoisomerization. Finite element implementation for plane stress problems is obtained through a self-defined material subroutine in ABAQUS FEA tool. Numerical simulations show that the light induced deformations of two dimensional specimens consist of contractions, expansions and bending in different directions. The stress distributions indicate that the driving force for the light induced bending is produced by the bending moment of the normal stress along the director, while the other stress components are much smaller for two dimensional beam shaped specimens. However, the shear stress of the soft LCE is generally nonzero under light illumination due to the inhomogeneity of the opto-mechanical effect. It can be concluded from the strain distributions that the transversal plane cross section could remain plane after deformation if the light intensity or the decay distance is not too small and the sample is in the deep nematic phase. However, the shear strain and in plane rotation are of the same order as the other strain components, and thus should not be neglected. This indicates that the classical simple bending assumptions such as the Euler–Bernoulli beam theory should not be directly applied to model the light induced bending of neo-classical liquid crystal elastomers due to the soft behavior of the materials.

1. Introduction

Liquid crystal elastomers (LCEs) are cross-linked polymers with liquid crystalline molecules. Thus they combine the elasticity with the liquid crystalline properties (Warner and Terentjev, 2003). When the temperature decreases to a critical value, the LCE changes from the isotropic phase to an anisotropic phase with liquid crystalline molecules aligning orderly along a specific direction, named as the director **n**. This critical temperature is called the nematic-isotropic (NI) phase transition temperature T_{ni} (de Gennes and Prost, 1994). After the phase transition, the LCEs will elongate in the direction **n**, and its elongation at temperature T can be well fitted by the following formula

$$\lambda_{i\to n} = 1 + \alpha(T_{ni} - T)^{\zeta}, \tag{1}$$

where α and ζ are positive constants. $\lambda_{i\to n}$ is a function of the difference between T_{ni} and T. Thus LCEs can be deformed not only by changing the temperature, but also by manipulating the NI transition temperature T_{ni}. The latter can indeed be achieved by photoisomerization of certain photochromic LCEs (Ikeda, 2003). Finkelmann et al. (2001) first introduced certain photochromic liquid crystal molecules into the LCEs. When photochromic liquid crystal molecules, e.g., azobenzenes, are added into LCEs, their photoisomerization under the light of a certain frequency will convert from the rod-like shape (called *trans*) to the kinked shape (called *cis*). The kinked liquid crystalline molecules will disturb the whole nematic order, decrease the NI transition temperature T_{ni} and finally lead to the macroscopic contraction of the stress-free samples (Finkelmann et al., 2001; Hogan et al., 2002) and accumulation of stress in the clamped ones (Cviklinski et al., 2002). This new kind of smart materials has a potential application in light controllable sensors and actuators.

When a light goes through a material, it will be absorbed. Classically, the Beer's exponential decay formula $I(y) = I_0\exp(-y/d)$ was often used with I_0 the light intensity distribution on the surface

* Corresponding author. Tel.: +86 21 55664171; fax: +86 21 65642742.
E-mail address: yzhuo@fudan.edu.cn (Y. Huo).
[1] Present address: School of Engineering and Applied Sciences, Harvard University, Cambridge, MA 02138, USA.

0020-7683/$ - see front matter © 2012 Elsevier Ltd. All rights reserved.
http://dx.doi.org/10.1016/j.ijsolstr.2012.05.031

and y the distance to the surface. The positive constant d is the characteristic distance of light decay due to absorption. Recently, a non-classical light absorption model was proposed by Corbett and Warner (2007) and Corbett and Warner (2008) for photochromic LCEs. The steady state light intensity is modified by $\ln[I(y)/I_0] + \tau\Gamma I_0(I(y)/I_0 - 1)) = -y/d$ (Eq. (2) in Corbett and Warner (2007) with slightly different notations). τ is the *cis* state lifetime and Γ is the absorption constant. $I(y)$ cannot be solved by elementary function but can be solved formally by using the Lambert W function $W_L(y)$ (called ProductLog function in Mathematica) as pointed out in Corbett and Warner (2008),

$$I(y) = \frac{1}{\tau\Gamma} W_L\left[\tau\Gamma I_0 \exp\left(\tau\Gamma I_0 - \frac{y}{d}\right)\right], \tag{2}$$

In any case, the light-induced strain in the LCE varies along the light propagation direction, which leads to the bending of the LCEs (Camacho-Lopez et al., 2004;Yu et al., 2003). Moreover, this light-induced heterogeneous configuration can result in other inhomogeneous material properties, such as stiffness (Jin et al., 2006).

So far, the research on the light-induced deformation of the liquid crystal elastomers has drawn wide attention. The light induced bending behavior of LCE thin films has been studied by several authors mostly with beam or plate models based on simple bending assumptions (Warner and Mahadevan, 2004; van Oosten et al., 2007; Jin et al., 2006; Jin et al., 2010a; Jin et al., 2010b; Zeng et al., 2010; Dunn, 2007; Dunn and Maute, 2009; Chen and He, 2008; He, 2007; Modes et al., 2010; Warner et al., 2010a,). However, the behavior of LCEs is in general very unusual due to the coupling between the elastomer and the liquid crystal moieties. In particular, the rotation of the LC director can have very strong effects on the mechanical response of the materials (Warner, 1999). Many studies have been conducted (Cesana and DeSimone, 2011; Jin et al., 2010b;Warner, 1999; Warner and Terentjev, 2003) to investigate the unusual soft or semi-soft behavior of LCEs. It is thus natural to ask whether the opto-mechanical behavior of LCEs will also be very unusual and may be affected strongly by the soft behavior. Consequently, it should be expected that some of the classical simple bending assumptions of Euler–Bernoulli beam theory (EBBT) or Kirchhoff–Love plate theory (KLPT) may fail to be satisfied. In addition, the papers (Conti et al., 2002a,b) represent some of the very first attempts to use FEA as a tool to understand the physics of LCEs. Due to the unusual material behaviors, it will benefit from using FEA to study the light induced bending behavior of LCEs.

In this paper, a stress–strain relation obtained by some of the present authors for soft LCEs (Jin et al., 2010b) will be applied to study the light induced bending behavior of photochromic LCEs. In Section 2, we shall first modify the constitutive equations obtained previously to include the effect of the photoisomerization. To simplify the analysis, linearized stress–strain relations are further obtained for infinitesimal deformations. The results indicate that although the shear stress in the plane perpendicular to the director vanishes identically for LCEs without light illuminations due to the soft behavior of the materials, it is proportional to the rotation of the director when the material is under light illumination. The proportional factor is the light induced changes of the effective length ratio of the polymer backbone and is generally rather small comparing to the other elastic moduli. Finite element analysis is then carried out for two dimensional specimens under the plane stress assumptions in Section 3. It is necessary to rescale the displacements and to input the unusual stress–strain relations by user defined material subroutine when we use the commercially available finite element software ABAQUS. Detailed analyses of the stress and strain states are given in Section 4. The kinematic hypotheses of EBBT will be tested in some details. The plane cross section assumption is generally valid for light induced bending except some extreme situations such as very weak light, very small decay distance and in the vicinity of the nematic-isotropic transition temperature. However, the normal plane cross section is no longer normal after deformations and the shear strain is not negligible even for very slender beam shaped specimen. The conclusions are summarized in Section 5.

2. Linearized stress–strain relation for LCEs under light illumination

2.1. Opto-mechanical constitutive relation

In this subsection, the effect of light is introduced into the nonlinear constitutive relations of photochromic LCEs obtained in Jin et al. (2010b). Let us make a brief review of it.

Choose the total free energy as the sum of the neo-classical elastic free energy f_{el} and the Landau de Gennes LC order free energy f_{nem}. The neo-classical elastic free energy per unit volume is

$$\rho_0 f_{el} = \frac{\mu}{2}\mathrm{Tr}(\mathbf{g}^{-1}\boldsymbol{\lambda}\mathbf{g}_0\boldsymbol{\lambda}^T) = \frac{\mu}{2}\mathrm{Tr}(\mathbf{g}^{-1}\mathbf{B}) \quad \text{with} \quad \mathbf{B} = \boldsymbol{\lambda}\mathbf{g}_0\boldsymbol{\lambda}^T, \tag{3}$$

where μ is the effective shear modulus and Tr $(\cdot)$ calculates the trace of the tensor inside. $\boldsymbol{\lambda}$ is the deformation gradient and $\mathbf{B} = \boldsymbol{\lambda}\mathbf{g}_0\boldsymbol{\lambda}^T$ is called the effective left Cauchy-Green tensor. $\mathbf{g}$ and $\mathbf{g}_0$ are called the metric tensors in the current and reference states, respectively. $\mathbf{g}$ defined there coincides with the commonly used shape tensor $\boldsymbol{l}$ but scaled to make it have unit determinant, i.e. $\boldsymbol{g} = \boldsymbol{l}\det(\boldsymbol{l})^{-1/3}$ with $\det(\mathbf{g}) = \det(\mathbf{g}_0) = 1$. In this paper, we only consider the case that $\det(\boldsymbol{l}) = \det(\boldsymbol{l}_0)$. More general cases can be referred to Warner and Terentjev (2003). In fact, it can be identified as the left Cauchy-Green tensor from the isotropic phase to the current nematic phase as shown in Jin et al. (2010b). It was found in Jin et al. (2010b) that the metric tensor $\mathbf{g}$ in the present configuration must be coaxial with the tensor $\mathbf{B}$ in order to minimize the free energy. Namely, when a deformation gradient $\boldsymbol{\lambda}$ is imposed on a LCE sample with the initial shape of the LC polymer backbone chains described by $\mathbf{g}_0$, the LC polymer chains will adjust their shape to make the current metric tensor $\mathbf{g}$ have the same eigenvector as the tensor $\mathbf{B} = \boldsymbol{\lambda}\mathbf{g}_0\boldsymbol{\lambda}^T$ so to minimize the elastic energy. Moreover, if $B_{1,2,3}$ are the eigenvalues of $\mathbf{B}$ corresponding to the eigenvectors $\mathbf{e}_{1,2,3}$ with the order $B_1 \leqslant B_2 \leqslant B_3$, the eigenvalues of $\mathbf{g}$, $g_{1,2,3}$ corresponding to the same eigenvectors must have the same order, i.e. $g_1 \leqslant g_2 \leqslant g_3$. Thus, we have

$$\mathbf{B} := \boldsymbol{\lambda}\mathbf{g}_0\boldsymbol{\lambda}^T = \sum_{i=1}^{3} B_i \mathbf{e}_i \otimes \mathbf{e}_i \quad \text{and} \quad \mathbf{g} := \boldsymbol{l}\det(\boldsymbol{l})^{-1/3} = \sum_{i=1}^{3} g_i \mathbf{e}_i \otimes \mathbf{e}_i. \tag{4}$$

The Cauchy stress σ is found to be coaxial with the effective left Cauchy-Green tensor as well and has the following expression for incompressible LCEs,

$$\boldsymbol{\sigma} = -p\mathbf{I} + \mu\mathbf{g}^{-1}\mathbf{B} = -p\mathbf{I} + \sum_{i=1}^{3} g_i^{-1} B_i \mathbf{e}_i \otimes \mathbf{e}_i, \tag{5}$$

where p is the hydrostatic pressure and $\mathbf{I}$ is the unit tensor.

Without considering the biaxiality of LCEs, the metric tensor $\mathbf{g}$ should be

$$\mathbf{g} = g_\perp \mathbf{I} + (g_{//} - g_\perp)\mathbf{n} \otimes \mathbf{n} = r^{-1/3}\mathbf{I} + (r^{2/3} - r^{-1/3})\mathbf{n} \otimes \mathbf{n}, \tag{6}$$

with $r = g_{//}/g_\perp = (R_{//}/R_\perp)^2$ the ratio of the effective length in the direction parallel and perpendicular to the director. $R_{//,\perp}$ are the radius of gyration of the polymer backbone. In fact, $\det(g) = g_{///}g_\perp^2 = 1$ is used to obtain the second equality in (6). Insert (6) into

(5), we obtain the stress-stretch relation for LCEs without biaxiality as,

$$\boldsymbol{\sigma} = -p\mathbf{I} + \mu r^{\frac{1}{3}}\left[\mathbf{B} - \left(1 - \frac{1}{r}\right) b_m \mathbf{n}\otimes\mathbf{n}\right], \tag{7}$$

where the current director $\mathbf{n}$ must be coincide with the eigenvector of the effective left Cauchy-Green tensor $\mathbf{B}$ with the largest eigenvalue, i.e.

$$\mathbf{n} = \mathbf{e}_3, b_{\mathrm{m}} = B_3 \quad \text{and} \quad \mathbf{B}\mathbf{n} = b_m\mathbf{n}. \tag{8}$$

Since $\mathbf{g}$ is the left Cauchy-Green tensor from the isotropic phase to the current nematic phase, we can relate its component along the director to $\lambda_{i\to n}$ by $r^{2/3} = \lambda^2_{i\to n}$. According to Eq. (1), we obtain the effective length ratio as

$$r = \begin{cases} (1 + \alpha(T_{ni} - T)^{\zeta})^3, & \text{for } T \leqslant T_{ni}; \\ 1, & \text{Otherwise} \end{cases} \tag{9}$$

Experimental and theoretical studies (Cviklinski et al., 2002; Finkelmann et al., 2001; Hogan et al., 2002; Ikeda, 2003) have shown that the shift of T_{ni} induced by light illumination can be calculated as

$$T_{ni} = T^0_{ni} - \beta n_c, \tag{10}$$

where T^0_{ni} is the NI phase transition temperature without illumination, β is a positive constant and n_c is the fraction of the cis isomers appeared due to photoisomerization process. It has been shown that under the illumination of light with suitable wavelength, the azo dyes will transform from the *trans* state to the *cis* state. Thus, n_c will increase under light illumination and approach a saturated value after long time irradiation,

$$n_c(I) = \frac{\tau\Gamma I}{1 + \tau\Gamma I}. \tag{11}$$

In this paper, the saturated case is considered for simplicity. When the LCEs are illuminated, since T_{ni} is a decreasing function of the light intensity I, the photoisomerization decreases the phase transition temperature T_{ni}. From Eq. (9), the effective length ratio r will be changed and thus produce a light induced deformation. Then by inserting Eq. (9) into the metric tensor (6), and inserting them all into the constitutive relation (7), we have introduced the light intensity into the nonlinear constitutive relations.

There can also be a temperature raise due to the light illumination (Dawson et al., 2011; Jiang et al., 2010). The effective length ratio (9) will be reduced as well and the following analysis can be applied in the same way.

2.2. Linearization of the stress–strain relation under light illuminations

The implementation of the neo-classical elastic energy of LCEs and its linearized version (DeSimone and Teresi, 2009; Agostiniani and DeSimone, 2011; Warner and Terentjev, 2003; de Gennes, 1982) for infinitesimal deformations into numerical calculations such as the finite element simulations is rather complicated. One major difficulty is the so-called soft behavior, the vanishing of certain shear modulus due to the free rotation of the directors (Warner et al., 1994; Olmsted, 1994). Thus, it is generally believed that in order to have nonsingular stiffness matrix, it is necessary either to use the modified semi-soft elastic energy (Verwey and Warner, 1995; Cesana and DeSimone, 2011) or to add higher order derivatives into the total energy such as the director gradient dependent Frank energy (de Gennes and Prost, 1994).

However, as shown very clearly by the following linearized stress–strain relations, the shear modulus will not vanish if the sample is under light illuminations. Thus, we can still use the simple neo-classical elastic energy to calculate the light induced bending behavior of LCEs. In addition to the consideration of the effect of light illumination, the main difference between the following linearization and the existing ones is that we are working directly on the stress–strain relation (7) obtained after the minimization of the total free energy.

For the anisotropic liquid crystal elastomers, the stress–strain relation (7) is linearized at the initial state (at r_0) : no light illumination and no deformation. It is easy to obtain the effective left Cauchy-Green tensor as defined in (3) in terms of the displacement gradient $\mathbf{H} = \boldsymbol{\lambda} - \mathbf{I} = \nabla\mathbf{u}$ as

$$\mathbf{B} = \mathbf{g}_0 + \mathbf{H}\mathbf{g}_0 + \mathbf{g}_0\mathbf{H}^T + \mathbf{H}\mathbf{g}_0\mathbf{H}^T, \tag{12}$$

Thus, $\mathbf{B} = \mathbf{g}_0$ when $\mathbf{H} = \mathbf{0}$ and for infinitesimal $\mathbf{H}$, the last term on the right, $\mathbf{H}\mathbf{g}_0\mathbf{H}^T$ is of the second order. Therefore, it seems natural define the effective infinitesimal strain tensor as

$$\boldsymbol{\varepsilon}_g = \frac{1}{2}\left(\mathbf{H}\mathbf{g}_0 + \mathbf{g}_0\mathbf{H}^T\right) = \frac{1}{2}(\boldsymbol{\varepsilon} g_0 + \mathbf{g}_0\boldsymbol{\varepsilon}) + \frac{1}{2}(\boldsymbol{\omega}\mathbf{g}_0 - \mathbf{g}_0\boldsymbol{\omega}), \tag{13}$$

where $\boldsymbol{\varepsilon} = (\mathbf{H} + \mathbf{H}^T)/2$ is the Cauchy strain and $\boldsymbol{\omega} = (\mathbf{H} - \mathbf{H}^T)/2$ is the skew symmetric part of the displacement gradient $\mathbf{H} = \nabla\mathbf{u}$, which is related to the infinitesimal rotation. So we can linearize the effective left Cauchy-Green tensor (12) by

$$\mathbf{B} \approx \mathbf{g}_0 + 2\boldsymbol{\varepsilon}_g. \tag{14}$$

Note that the above effective strain $\boldsymbol{\varepsilon}_g$ and effective $\mathbf{B}$ can depend on both the symmetric part and the skew symmetric part of the displacement gradient if the initial metric tensor $\mathbf{g}_0$ is not the identical tensor, i.e. the initial configuration is not isotropic.

Suppose that the director in the current configuration changes from the initial configuration by an infinitesimal amount as well,

$$\mathbf{n} = \mathbf{n}_0 + \delta\mathbf{n}, \tag{15}$$

only considering the linear terms, and we have $1 = \mathbf{n}\cdot\mathbf{n} = 1 + \mathbf{n}_0\cdot\delta\mathbf{n}$, so $\mathbf{n}_0\cdot\delta\mathbf{n} = 0$. Substitute Eqs. (14), (15) into the third formula of Eq. (8) and inner product both sides by $\mathbf{n}_0$, we have

$$\begin{aligned}&\mathbf{n}_0\cdot\mathbf{g}_0\mathbf{n}_0 + 2\mathbf{n}_0\cdot\boldsymbol{\varepsilon}_g\mathbf{n}_0 + \mathbf{n}_0\cdot\mathbf{g}_0\delta\mathbf{n} + 2\mathbf{n}_0\cdot\boldsymbol{\varepsilon}_g\delta\mathbf{n} \\ &\quad = b_m(\mathbf{n}_0\cdot\mathbf{n}_0 + \mathbf{n}_0\cdot\delta\mathbf{n})\end{aligned}$$

Since $\mathbf{g}_0 = r_0^{-1/3}\mathbf{I} + \left(r_0^{2/3} - r_0^{-1/3}\right)\mathbf{n}_0\otimes\mathbf{n}_0$ for initially nematic state, $\mathbf{n}_0\cdot\mathbf{n}_0 = 1$, $\mathbf{n}_0\cdot\delta\mathbf{n} = 0$ and neglect the second order term $\mathbf{n}_0\cdot\boldsymbol{\varepsilon}_g\delta\mathbf{n}_0$, we can obtain

$$b_m = r_0^{\frac{2}{3}} + 2\mathbf{n}_0\cdot\boldsymbol{\varepsilon}_g\cdot\mathbf{n}_0. \tag{16}$$

Inserting the above equation and (14) and (15) back to the third formula of Eq. (8) and neglect the second order term $\boldsymbol{\varepsilon}_g\delta\mathbf{n}$, we can obtain the director rotation as

$$\delta\mathbf{n} = \frac{2r_0^{\frac{1}{3}}}{r_0 - 1}(\boldsymbol{\varepsilon}_g\cdot\mathbf{n}_0 - (\mathbf{n}_0\cdot\boldsymbol{\varepsilon}_g\cdot\mathbf{n}_0)\mathbf{n}_0). \tag{17}$$

We substitute Eq. (17) into Eq. (15) and insert it into (7) together with (14) and (16) to obtain the following linearized stress–strain relation

$$\begin{aligned}\boldsymbol{\sigma} = &-\tilde{p}\mathbf{I} + \mu\left(\frac{r_0}{r}\right)^{2/3}\frac{r_0 - r}{r_0}\mathbf{n}_0\otimes\mathbf{n}_0 \\ &+ 2\mu r^{1/3}\left\{\boldsymbol{\varepsilon}_g + \frac{r-1}{r_0-1}\frac{1+r_0}{r}(\mathbf{n}_0\cdot\boldsymbol{\varepsilon}_g\cdot\mathbf{n}_0)\mathbf{n}_0\right. \\ &\left.\otimes\mathbf{n}_0 - \frac{r_0}{r}\frac{r-1}{r_0-1}\left[\mathbf{n}_0\otimes(\boldsymbol{\varepsilon}_g\cdot\mathbf{n}_0) + (\boldsymbol{\varepsilon}_g\cdot\mathbf{n}_0)\otimes\mathbf{n}_0\right]\right\}.\end{aligned} \tag{18}$$

Note that second order terms in $\boldsymbol{\varepsilon}_g$ and $\delta\,\mathbf{n}$ are all neglected, the expression for $\mathbf{g}_0$ is inserted and the constant $\tilde{p} = p - \mu(r/r_0)^{\frac{1}{3}}$.

By using Eq. (13), we can rewrite the above stress–strain relation in terms of the Cauchy strains (symmetric part) $\boldsymbol{\varepsilon}$ and the rotation (skew symmetric part) $\boldsymbol{\omega}$ as

$$\begin{aligned}\boldsymbol{\sigma} = & -p\mathbf{I} + 2\mu\left(\frac{r}{r_0}\right)^{1/3}\left\{\boldsymbol{\varepsilon} - \left[1 - \frac{r_0+1}{2(r_0-1)}\frac{r_0-r}{r}\right][\mathbf{n}_0 \right.\\ & \otimes\left(\boldsymbol{\varepsilon}\cdot\mathbf{n}_0) + (\boldsymbol{\varepsilon}\cdot\mathbf{n}_0)\otimes\mathbf{n}_0] + \frac{2r_0}{r}\frac{r-1}{r_0-1}(\mathbf{n}_0\cdot\boldsymbol{\varepsilon}\cdot\mathbf{n}_0)\mathbf{n}_0\\ & \left.\otimes\mathbf{n}_0 + \frac{r_0-r}{2r}[\mathbf{n}_0\otimes\mathbf{n}_0 + \mathbf{n}_0\otimes(\boldsymbol{\omega}\cdot\mathbf{n}_0) + (\boldsymbol{\omega}\cdot\mathbf{n}_0)\otimes\mathbf{n}_0]\right\}. \end{aligned} \quad (19)$$

The last term that is proportional to the light induced contraction r_0-r will produce a non-vanishing shear modulus as shown clearly in the following plane stress case. We close this subsection by pointing out that the shear stress on the surface with the director $\mathbf{n}_0$ as the normal is not zero but proportional to r_0-r and the rotation of the director $\delta\mathbf{n}$ of (17) as

$$\begin{aligned}\tau_{\mathbf{n}_0} &= \mu\left(\frac{r}{r_0}\right)^{1/3}\frac{r_0-r}{r}\delta\mathbf{n}\\ &= 2\mu r^{-2/3}\frac{r_0-r}{r_0-1}[\boldsymbol{\varepsilon}_g\cdot\mathbf{n}_0 - (\mathbf{n}_0\cdot\boldsymbol{\varepsilon}_g\cdot\mathbf{n}_0)\mathbf{n}_0]\\ &= \mu\left(\frac{r}{r_0}\right)^{1/3}\\ &\quad\times\frac{r_0-r}{r}\left\{\boldsymbol{\omega}\cdot\mathbf{n}_0 + \frac{r_0+1}{r_0-1}[\boldsymbol{\varepsilon}\cdot\mathbf{n}_0 - (\mathbf{n}_0\cdot\boldsymbol{\varepsilon}\cdot\mathbf{n}_0)\mathbf{n}_0]\right\}. \end{aligned} \quad (20)$$

Thus, the material behavior is rather different under light illumination. Namely, the shear stress vanishes identically when there is no light, i.e. $r \equiv r_0$. This is often referred as the soft behavior (Cesana and DeSimone, 2011; Jin et al., 2010b; Warner, 1999; Warner and Terentjev, 2003) as predicted by the neo-classical elastic energy. However, the light induced change of the effective length ratio $r \neq r_0$ will produce a nonzero shear stress as indicated by (20). The first equation in (20) implies also that the rotation of director is free when $r \equiv r_0$ but will be proportional to the shear stress if $r \neq r_0$.

2.3. Constitutive equations for plane stress problem

The above stress–strain relation (19) for infinitesimal deformations is still rather complex. In order to demonstrate how to implement it into finite element calculations, we shall consider in this paper only plane problems for simplification. The full three dimensional solutions are under construction.

As shown in Fig. 1, we consider a LCE beam, with length $2L$, height h and width w. The director is parallel with x direction, i.e., $\mathbf{n}_0 = (1,0,0)^T$ and it is illuminated by unpolarized light along the y direction from the bottom. The decayed light intensity (2) causes the inhomogeneous light-induced contraction along the director, the x-axis, which induces the bending in the x-y plane. Due to the Poisson effect, an inhomogeneous extension will appear along the z-axis, which further causes the bending in the y-z plane as discussed by Warner et al. (2010a,Warner et al. (2010).

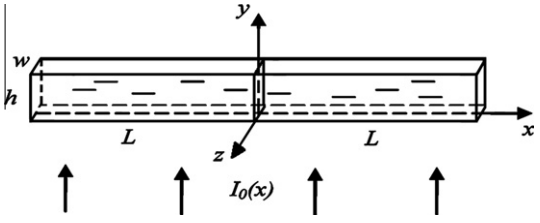

Fig. 1. The schematic of the beam shaped specimen under the upward unpolarized light, with the LC director parallel with x direction.

However, if the specimen is very thin ($w \ll h$ and L) and we are concerned with the deflection in the x-y plane at $z = 0$, a plane stress assumption should be a reasonable approximation.

Thus, under the plane stress assumption, we would have $\sigma_{zz} = \sigma_{xz} = \sigma_{yz} = 0$ and the in-plane displacements as $(u(x,y), v(x,y))$. Due to the incompressibility $tr(\boldsymbol{\varepsilon}) = 0$, we have $\varepsilon_{zz} = -(\varepsilon_{xx} + \varepsilon_{yy})$ with $\varepsilon_{xx} = u_{,x}$, $\varepsilon_{yy} = v_{,y}$ and $\varepsilon_{zz} = w_{,z}$ the geometric equations for the Cauchy strain.

By Eq. (19), we can obtain $p = -2\mu(r/r_0)^{1/3}(\varepsilon_{xx} + \varepsilon_{yy})$. Thus, we can obtain the following stress–strain relation for plane stress problems

$$\begin{cases}\sigma_{xx} = \frac{E_{//}}{1-sv^2}\left(\left(\varepsilon_{xx} - \varepsilon^r_{xx}\right) + sv\left(\varepsilon_{yy} - \varepsilon^r_{yy}\right)\right)\\ \sigma_{yy} = \frac{E_{\perp}}{1-sv^2}\left(\left(\varepsilon_{yy} - \varepsilon^r_{yy}\right) + v\left(\varepsilon_{xx} - \varepsilon^r_{xx}\right)\right)\\ \sigma_{xy} = \sigma_{yx} = 2G_{eff}\varepsilon^g_{xy} = 2G\varepsilon_{xy} - 2\overline{G}\omega_{xy}\end{cases}, \quad (21)$$

where the effective shear strain is $\varepsilon^g_{xy} = \left(r_0^{-1/3}u_{,y} + r_0^{2/3}v_{,x}\right)/2$ as shown in Eq. (13). The Cauchy shear strain and in plane rotation are defined as $\varepsilon_{xy} = (u_{,y} + v_{,x})/2$ and $\omega_{xy} = (u_{,y} - v_{,x})/2$, respectively. The light induced strains are

$$\varepsilon^r_{xx} = -\frac{r_0-r}{2r_0+r} \quad \text{and} \quad \varepsilon^r_{yy} = -v\varepsilon^r_{xx}. \quad (22)$$

The elastic constants are

$$\begin{aligned}E_{//} &= \mu\left(\frac{r}{r_0}\right)^{1/3}\frac{r+2r_0}{r}, \quad E_{\perp} = 2\mu\left(\frac{r}{r_0}\right)^{1/3}\frac{r+2r_0}{r+r_0}, \quad v\\ &= \frac{1}{2}, \quad s = \frac{E_{\perp}}{E_{//}} = \frac{2r}{r+r_0} \quad G_{eff} = \mu r^{-2/3}\frac{r_0-r}{r_0-1}, \quad 2G\\ &= \left(r_0^{2/3} + r_0^{-1/3}\right)G_{eff}, \quad 2\overline{G} = \left(r_0^{2/3} - r_0^{-1/3}\right)G_{eff}. \end{aligned} \quad (23)$$

The first two stress–strain relations in (21) for the normal stress components look very similar to the linearly thermoelastic Hooke's law with the thermal strain replaced by the anisotropic opto strains given by (22). However, the constitutive relation for the shear stress is very unusual. Firstly, the effective shear modulus G_{eff} together with G and $\overline{G}$ are only nonzero under light illuminations. At the first order, all the three moduli and the light induced strain are proportional to the difference of the effective length ratio $r_0 - r$, which is induced by the light irradiation. Secondly, the Cauchy shear stress is not proportional to the Cauchy shear strain, but depends on the in plane rotation as well. This very special constitutive equation for the shear stress is due to the ability of free rotation of the liquid crystal director (17) and will have very strong effect on the opto-mechanical behavior of LCEs as will be shown next.

The effective Young's moduli $E_{//,\perp}$ depend on the effective length ratio r and are affected by the light illuminations as well. Therefore, the LCE material under light illumination becomes a functional gradient material since the light induced change of the effective length ratio $r_0 - r$ (Eqs. (9)–(11)) depends on the space varying light intensity (Eq. (2)). More discussions can be found in (Jin et al., 2006). Moreover, the light induced decrease of the effective length ratio r implies that $E_{//} > E_{\perp}$, the light induced anisotropy. As observed in experiments and discussed in several theoretical works (Zeng et al., 2010), the elastic moduli of single domain LCEs are anisotropic and depend strongly on the temperature. However, it is necessary to take into consideration that the stress induces biaxiality of the liquid crystal molecules in order to obtain this anisotropy. In the present paper, the biaxiality is neglected for simplicity. Thus, the elastic moduli are taken as isotropic under mechanical loading and the anisotropy is induced by the light illumination.

3. Finite element simulations of light-induced bending of free-standing LCE specimen

3.1. Finite element implementation of the plane stress problem under light

We can obtain the governing equations for the displacements $(u(x,y), v(x,y))$ by inserting the geometric equation and the constitutive Eq. (21) of the plane stress problem into the stress equilibrium equations. The weak form of the governing equations can be obtained through the standard procedures as well. However, because the constitutive Eq. (21) is nonstandard due to the presence of the skew symmetric part of the displacement gradient, the in plane rotation ω_{xy}, the finite element implementation is not so straightforward. We have found that the following scaling of the displacement fields and the corresponding strains for an initially homogeneous LCE sample with constant r_0 will give a standard stress–strain relation,

$$\bar{u}(x,y) = r_0^{-1/3}u(x,y), \quad \bar{v}(x,y) = r_0^{2/3}v(x,y)$$
$$\bar{\varepsilon}_{xx} = r_0^{-1/3}\varepsilon_{xx}, \quad \bar{\varepsilon}_{yy} = r_0^{2/3}\varepsilon_{yy}, \quad \bar{\varepsilon}_{xy} = r_0^{-1/3}((r_0+1)\varepsilon_{xy} - (r_0-1)\omega_{xy}). \tag{24}$$

It is worthwhile to point out that the above scaled shear strain $\bar{\varepsilon}_{xy}$ is identical to the effective shear strain ε^g_{xy} obtained from (13). The constitutive Eq. (21) can then be rewritten into the following matrix form

$$\{\sigma\} = [\bar{D}]\{\bar{\varepsilon}\} - \{\sigma_r\}, \tag{25}$$

where the stress and scaled strain vectors are

$$\{\sigma\}^T = \{\sigma_{xx}, \sigma_{yy}, \sigma_{xy}\} \quad \text{and} \quad \{\bar{\varepsilon}\}^T = \{\bar{\varepsilon}_{xx}, \bar{\varepsilon}_{yy}, 2\bar{\varepsilon}_{xy}\} = \left\{\frac{\partial \bar{u}}{\partial x}, \frac{\partial \bar{v}}{\partial y}, \frac{\partial \bar{u}}{\partial y} + \frac{\partial \bar{v}}{\partial x}\right\}. \tag{26}$$

The effective stiffness matrix and the opto stress are

$$[\bar{D}] = \frac{r_0^{1/3}E_{//}}{1-sv^2}\begin{bmatrix} 1 & sv/r_0 & 0 \\ sv & s/r_0 & 0 \\ 0 & 0 & s_G/r_0^{1/3} \end{bmatrix} \quad \text{and} \quad \{\sigma_r\} = \begin{Bmatrix} -E_{//}\varepsilon^r_{xx} \\ 0 \\ 0 \end{Bmatrix}, \tag{27}$$

with $s_G = G_{eff}/(E_{//}/(1-sv^2))$. Note that the effective stiffness matrix $\bar{D}$ is generally not symmetric when LCE is in the liquid crystal phase with $r_0 > 1$. Moreover, since we have assumed that the ratio of the light induced strain $v^r = -\varepsilon^r_{yy}/\varepsilon^r_{xx}$ is the same as the elastic Poison ratio $v = 1/2$, the opto stress in the y-axis, which is perpendicular to the director $\mathbf{n}_0$, is identically zero. There are some evidences that for heavily cross-linked liquid crystal polymers in the glassy phase, the two ratios may not be the same (Warner et al., 2010a,). Then, it is possible that there is an opto stress component in the directions perpendicular to $\mathbf{n}_0$.

Now, we can follow the standard procedure by using the above scaled displacements and scaled strains (24) to obtain the weak formulation of the stress equilibrium equations for a free standing two dimensional specimen Ω under light illumination as

$$\int_\Omega [\bar{D}]\{\bar{\varepsilon}\}\cdot\{\delta\bar{\varepsilon}\}dxdy = \int_\Omega \{\sigma_r\}\cdot\{\delta\bar{\varepsilon}\}dxdy, \tag{28}$$

where

$$\{\delta\bar{\varepsilon}\}^T = \{\delta\bar{\varepsilon}_{xx}, \delta\bar{\varepsilon}_{yy}, 2\delta\bar{\varepsilon}_{xy}\} = \left\{\frac{\partial\delta\bar{u}}{\partial x}, \frac{\partial\delta\bar{v}}{\partial y}, \frac{\partial\delta\bar{u}}{\partial y} + \frac{\partial\delta\bar{v}}{\partial x}\right\}. \tag{29}$$

Thus, (28) is the standard weak form of plane stress problem with a special stress–strain relation defined in Eq. (25). Therefore, any commercial finite element method (FEM) software can be used to implement the above plane stress problem provided that it is possible to input user defined material model. The finite element tool ABAQUS will be utilized in the following simulation with a self-defined material subroutine UMAT for the stress–strain relation Eq. (25).

3.2. Light induced contractions of a rectangular specimen

Based on the plane stress assumption and in view of the symmetry in the x direction of this specimen, only half of the beam is considered here and the model has been simplified into a two dimensional plane with $z = 0$ (the middle plane in the z direction). The two dimensional rectangular specimen with symmetric boundary condition on the left are shown in Fig. 2 together with specified coordinate system x-y. The reason why we have set the y-axis starting from the bottom surface is simply because we want to use formula (2) for calculation the light absorption. Quadrilateral meshes with $\Delta x/\Delta y = 2$ are chosen in order to prevent the deformity of the elements.

The relevant parameters for the calculation of the effective length ratio r of (9) are taken from the experiment in the paper of Hogan et al. (2002) as

$$T^\circ_{ni} = 340K, \quad \alpha = 0.22, \quad \zeta = 0.195, \quad \beta = 11.8K. \tag{30}$$

The parameters for the light absorption in (2) and (11) are scaled in the dimensionless light intensity $i_0 = \tau\Gamma I_0$. In this section, the temperature is fixed at the room temperature $T = 298$ K. Thus the material is in the deep nematic phase.

Let us first consider an extreme case that the decay distance is very large, $d/h \gg 1$. From (2), the light intensity will be approximately constant along the height, $I(y) \approx I_0$. Thus, the *cis* isomer fraction in Eq. (11) and the effective length ratio in Eqs. (9) and (10) are constants as $n_c(i_0)$ and $r(i_0)$, respectively, with the dimensionless light intensity $i_0 = \tau\Gamma I_0$. Therefore, the light induced strains in Eq. (22) and all the elastic moduli in Eq. (23) are constants as well. For a free standing rectangular specimen as shown in Fig. 2, the stress vanishes identically in the sample and the specimen is subjected to a homogeneous contraction in the x direction and a homogeneous expansion in the y direction as $\varepsilon_{xx} \approx \varepsilon^r_{xx}(i_0)$ and $\varepsilon_{yy} \approx \varepsilon^r_{yy}(i_0) = -v\varepsilon^r_{xx}(i_0)$. The displacements are linear functions as

$$u(x,y) = \varepsilon^r_{xx}(i_0)x \quad \text{and} \quad v(x,y) = -v\varepsilon^r_{xx}(i_0)y. \tag{31}$$

The first report of opto mechanical effect (Finkelmann et al., 2001) is exactly the homogeneous contraction induced by UV light for LCEs with dilute azo dyes, thus very small light absorption and very large decay distances are considered in this example. The time evolution of the light induced contraction resulted from the dynamics of the photoisomerization process as observed in the experiments (Finkelmann et al., 2001; Hogan et al., 2002) could be taken into account if we consider the dynamical equations proposed in Corbett and Warner (2008) in place of the steady state solutions (2) and (11). For simplicity, we confine ourselves in this paper to study only the steady states and leave the dynamical effects to our future work.

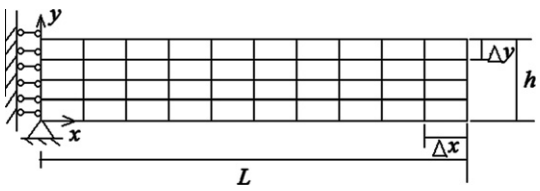

Fig. 2. The schematic of the finite element model of the specimen and the symmetric boundary condition.

The FEM calculations in ABAQUS are performed with $d/h = 100$ and a mesh of 10 nodes in both directions for a sample with $L/h = 1$. The deformed specimen and the contour maps of the displacements are shown in Fig. 3.

It is obvious that the sample contracted in length and expanded in heights. Moreover, the horizontal displacement $u(x,y)$ is constant at any given height (Fig. 3a), thus independent on y. And the vertical displacement $v(x,y)$ is constant along the horizontal cross sections (Fig. 3b) and is independent on x. The linear dependences of the displacements $(u(x), v(y))$ on the remaining variables are shown by Fig. 3 as well with the dots from FEM calculations and the continuous curves obtained by Matlab calculations from the above analytical solutions of (31). They agree with each other very well.

Due to the nonlinearity in (11) of the photoisomerization process and in (1) and (9) of the nematic-isotropic transition process of photochromic LCEs, the light induced contraction decreases nonlinearly with the light intensity as shown in Fig. 4. Again, the FEM results agree with the analytical solutions very well for both the contractions in length and expansions in height.

3.3. Bending of beam shaped specimens under uniform light illuminations

When the density of the photochromic dyes is large enough, the decay distance d/h becomes small enough such that the light will be absorbed strongly along the propagation. After a sufficiently long illumination time, the photoisomerization process goes to a steady state. Then, the decrease of the light intensity $i(y)$ can be calculated by (2) and the *cis* isomer density $n_c(y)$ is given by (11). From (9) and (10), the effective length ratio r varies along the height as well. As shown in Fig. 5(a) for $d/h = 1$, the light intensity decays very strongly along the height. Fig. 5(b) depicts that the cis isomer is larger for stronger light and decreases along the height similarly as the light intensity of Fig. 5(a). The effective length ratio r is lowered by the light illumination as shown in Fig. 5(c). The reduction is larger at shorter distance and for stronger light. Thus,

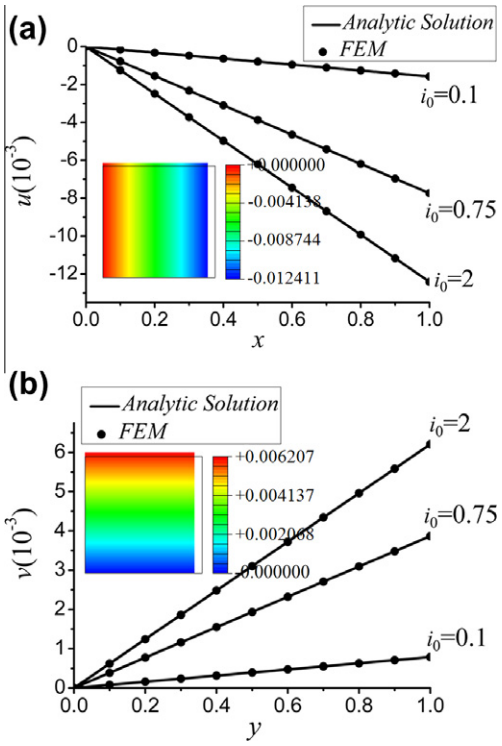

Fig. 3. (a) The distribution of the horizontal displacement $u(x, y = h/2)$ along the length of the beam. (b) The distribution of the vertical displacement $v(x = L/2, y)$ along the height of the beam, with $d/h = 100$, $L/h = 1$. The deformation and the contour maps of displacement for $L/h = 1$, $i_0 = 2$ from FEM are attached in the figures.

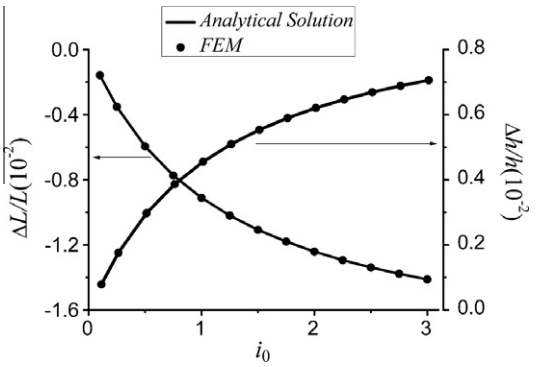

Fig. 4. The variations of light induced deformation $\Delta L/L = u(L, h/2)$ and $\Delta h/h = v(L/2, h)$ for different initial light intensities.

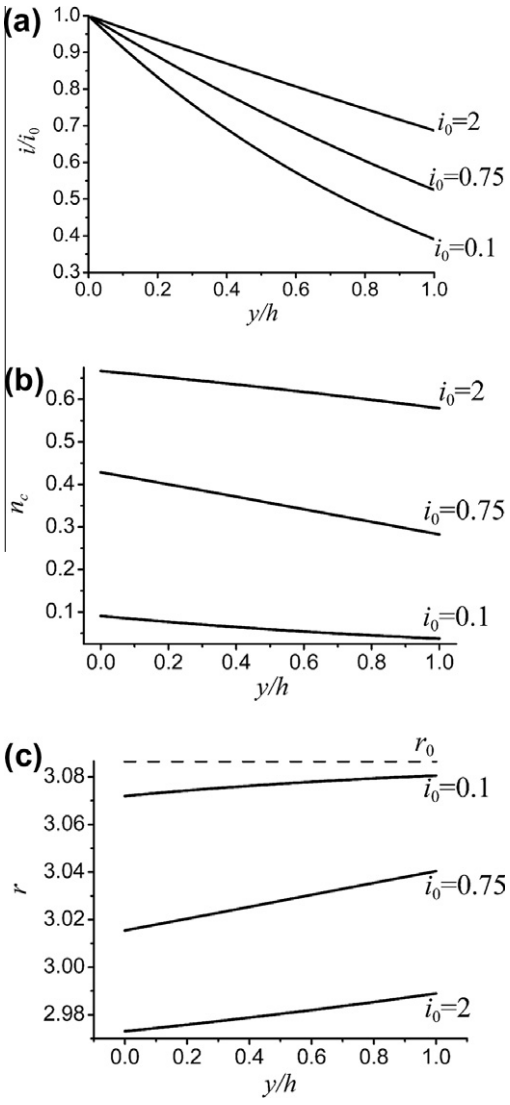

Fig. 5. The variations of (a) light intensity, (b) *cis* isomer density and (c) effective length ratio through the height with $d/h = 1$, for different initial light intensities $i_0 = 0.1, 0.75, 2$.

the effective length ratio r becomes space varying after the light illumination. From Fig. 5 and the formula (2), we observe that very weak light seems to decrease more closely to the classical Beer's exponential decay law, but stronger light will follow a more linearly decreasing function as observed in Corbett and Warner (2008). It seems that the *cis* isomer density and the effective length ratio follow the same trends.

To perform the FEM calculation, we need to test the convergence of the mesh shown in Fig. 2. Fig. 6 shows how the maximal Von Misses stress converges with the increase of the number of nodes for a slender beam with $L/h = 10$. The result indicates that the mesh is convergent and we should choose at least $N_y = 200$ nodes along the height direction and then $N_x = 1000$ nodes in the x direction for $L/h = 10$ to maintain the ratio of the mesh $\Delta x/\Delta y = 2$. It is worthwhile to point out that the convergence is particularly slow for the case $i_0 = 0.75$ due to its rather complex stress distribution along the beam height as will be shown in the next section.

As shown in Fig. 7, the straight beam becomes obviously shorter, thicker and is bended towards the light incoming direction after the light illumination. The light induced contraction is still rather large for the sample with $d/h = 1$. However, the light induced bending is visible unlike the previous examples with very large decay distances. It is a little surprising that the transversal cross lines seem to remain straight after deformation, but not normal to the deformed middle line any more. This means that there should be a relatively large shear effect and EBBT cannot be applied directly. More discussions will be given in the next section.

Here, we shall first study the light induced deflections, namely, the deflection curve of the middle line of the beam with $y = h/2$, $v(x,h/2)$. The scaled deflection curves $\hat{v}(x) = hv(x,h/2)/L^2$ of the middle line $y = h/2$ are shown in Fig. 8(a) for slender beam $L/h = 10$ and very short beam $L/h = 1$. They seem identical and can be well fitted by the following quadratic function which is also shown in Fig. 8(a) by continuous curves.

$$\hat{v}_0(x) = -\frac{1}{2}k_{eff}\left(\frac{x}{L}\right)^2 = -\frac{1}{2}\frac{h}{R_{eff}}\left(\frac{x}{L}\right)^2, \tag{32}$$

where $k_{eff} = h/R_{eff}$ is the effective curvature of the deflection and is listed in Table 1.

It is obvious from Table 1 that the bending curvature for $i_0 = 0.75$ is larger than $i_0 = 2$. Thus, a stronger light does not necessarily produce a larger deflection. This non-monotonic dependence of the bending curvature on the light intensity is shown more clearly in Fig. 8(b). Namely, k_{eff} increases firstly with the light intensity and decreases after arriving at a maximal value k_{eff}^M at certain critical light intensity i_0^M. The maximal curvature and the critical intensity are the same for different length L/h, but they depend strongly on the decay distance d/h as indicated by Fig. 8(b). Similar behavior is also observed in light induced bending models using simple beam theory (Jin et al., 2010a). As discussed in some details there, the reason for the non-monotonicity is because the bending magnitude does not depend directly on the magnitude of the light-induced strains, but depends on the gradient of the light-induced strain distributions along the beam height. While the light-induced strain magnitude does increase with the light intensity, the gradient does not. This is also confirmed by the present FEM calculation as will be shown more clearly by the strain distributions in the next section.

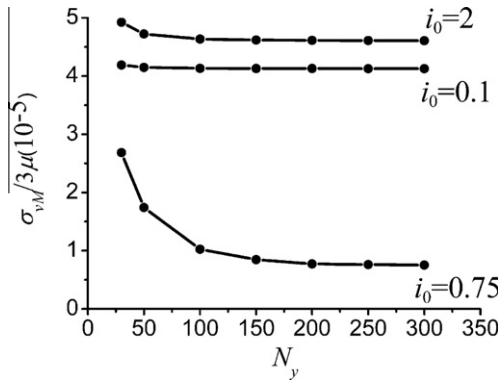

Fig. 6. The maximum von Misses stress versus different node numbers in y direction, which shows the convergence trend of the mesh in the slender beam with $L/h = 10$.

3.4. Bending of the specimen under non-uniform light illuminations

The finite element model developed here can be used to simulate the bending of the 2D beam illuminated by light with a distributed light intensity $I_0(x)$. Some examples will be shown in the following. In fact, even a time varying light intensity $I_0(t,x)$ can be applied as well, provided that the dynamical equation of the photoisomerization process must be considered in place of the steady state Eq. (11) for the *cis* fraction density.

Consider a laser spot with a Gaussian distributed intensity (Jin et al., 2011; Saleh and Teich, 1991)

$$I_0(x) = I_m \exp\left(-\frac{2(x-b)^2}{a^2}\right), \tag{33}$$

where I_m is the intensity at the center $x = b$ with $-L < b < L$ and the positive constant a is the half width of the distribution of the electric field on the surface. Fig. 9 depicts the bending of a slender specimen with $L/h = 10$ under the distributed light illuminations from the bottom with $I_{01}(x)(b_1 = 0, a_1/h = 1)$ and from the top with $I_{02}(x)(|b_2| = 0, a_2 = 1)$

Fig. 9(a) depicts that the whole beam contracts in length. The light induced expansions in height occur in the portions that are illuminated by $I_{01}(x)$ and $I_{02}(x)$. The beam remains quite straight for large $x > (|b_2| + a_2)$, where the light intensity is very small. Therefore, bending shape can be designed by suitable direction and distribution of light illumination.

4. Characteristics of the stress and strain distributions under uniform light illumination

The above FEM results indicate that due to the very special constitutive relations of photochromic LCEs, light illumination can induce deformations of the sample. For slender beam shaped specimen with the LC director along the length direction, the light illumination of the beam surface will induce a contraction in the length direction. In the other direction, the specimen will expand and bend toward the light incoming direction. The deflection curve of a free standing beam seems to be a quadratic function in accordance to the prediction of the simple beam theory. However, the deformation of the specimen indicates that the classical simple beam theory is violated, since the transversal normal cross section does not remain normal after the deformation. In order to better understand the above unusual opto-mechanical behavior of LCEs, we shall consider the stresses and strains of the sample in some details. Only uniform illumination of free standing samples will be considered in this section.

4.1. The stress distributions in 2-dimensional specimen bended under light

As shown in Fig. 10, the magnitude of the normal stress in the length direction σ_{xx} is at least one magnitude larger than all the

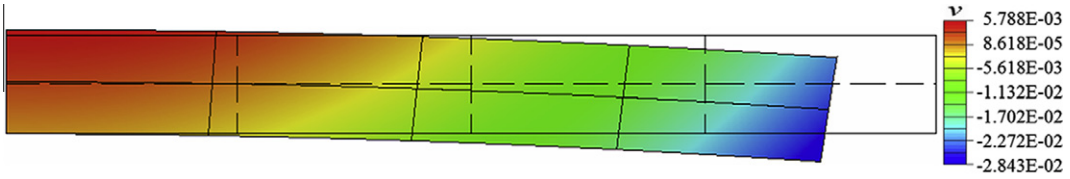

Fig. 7. The result of the vertical displacement $v(x,y)$ for $L/h = 10$, $i_0 = 2$.

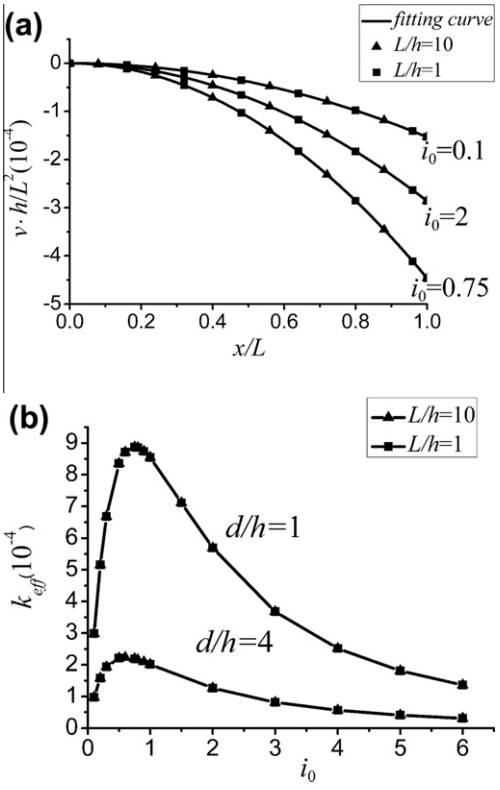

Fig. 8. (a) Normalized vertical displacement of the middle line versus different initial light intensities for $L/h = 10$ and 1. (b) The effective curvature with respect to various initial light intensities for different decay distances.

Table 1
The effective curvatures, slopes and contractions for different light intensities.

i_0	$k_{eff}(10^{-4})$	$k_\varepsilon(10^{-4})$	ε^0_{xx} (%)
0.1	2.9848	9.2110	−0.1054
0.75	8.8723	27.362	−0.6376
2	5.6878	17.551	−1.1577

other stress components even for very short beam with $L/h = 1$. Moreover, the maximal values for the other two stress components σ_{yy} and σ_{xy} are achieved near the free end at $x = L$, mainly due to the boundary effect while σ_{xx} is large in the middle portion and zero at $x = L$ as shown by Fig. 11. Comparing the slender and short beams, we find that the magnitudes of the stresses are generally smaller in shorter beam due to the free boundary effect.

Thus, we may conclude that σ_{xx} is the main driving stress for the light induced bending of the beam shaped specimen. The distribution of σ_{xx} along the height direction is shown in Fig. 12. It is clear that σ_{xx} varies non-monotonically along the height. Depending on the light intensity i_0, there are three very different types of stress distributions. Type I: tension near the lower and upper surface, but compression in the middle as shown by Fig. 12(a). Thus, there are two zero stress positions. Type II: two tension regions and two

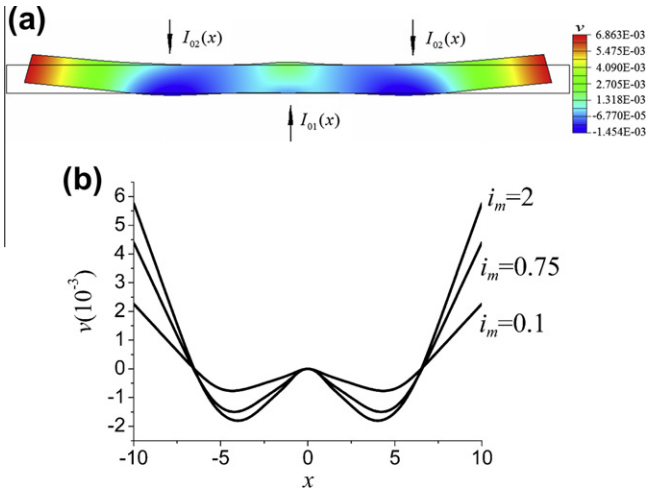

Fig. 9. (a) The bending shape and the contour plot of the vertical displacement of the whole beam under the upward laser I_{01} and the downward laser I_{02}, with $i_m = 2$. (b) Vertical displacement of the middle line with different initial light intensities.

compression regions spaced in between. There are three zero stress positions. Type III: one tension region and two compression regions with two zero stress positions.

In the classical EBBT, the stress σ_{xx} is assumed to be linear in the height direction. There is only one zero stress plane and is often called neutral plane. Thus, the stress distribution of the light induced bending of LCEs is very different from the classical bending. This phenomenon was already noticed by using extended EBBT (Jin et al., 2010a; Warner et al., 2010a; Warner et al., 2010b; Warner et al., 2011). Which one of the above three types should appear is determined by the light intensity i_0 and the decay distance d/h as discussed in details in Jin et al. (2010a). Roughly speaking, weak light will induce Type I and strong light induces Type III. Type II is produced by some intermediate light intensities.

4.2. The normal strain distributions

The normal strains ε_{xx} and ε_{yy} inside the sample are shown in Fig. 13 for $L/h = 1$ with $i_0 = 2$. It seems that they are both homogeneous along the beam length.

Their distributions along the height direction are shown in Fig. 13 for three different light intensities. It seems from Fig. 13(a) that the contraction strain ε_{xx} are identical for long ($L/h = 10$) and short ($L/h = 1$) beams and can be well fitted by a linear function

$$\varepsilon_{xx} = \varepsilon^0_{xx} + k_\varepsilon(y/h - 1/2). \tag{34}$$

This linearity is consistent with the observation from Fig. 7 that the transversal cross lines remained straight after deformation. The fitted values of ε^0_{xx} and k_ε are listed in Table 1.

As shown by Table 1, while the average contraction of the beam ε^0_{xx} is larger in magnitude for stronger light, the slope k_ε is obviously not monotonic. Moreover, according to EBBT, the slope k_ε

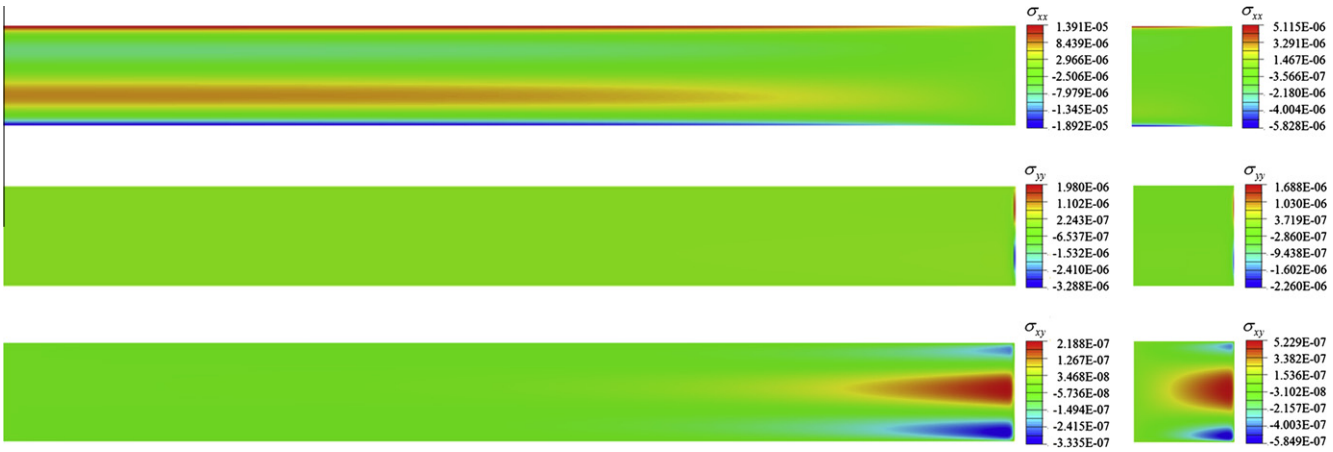

Fig. 10. Contour plots of σ_{xx}, σ_{yy} and σ_{xy} of the beam with the initial light intensity $i_0 = 0.75$.

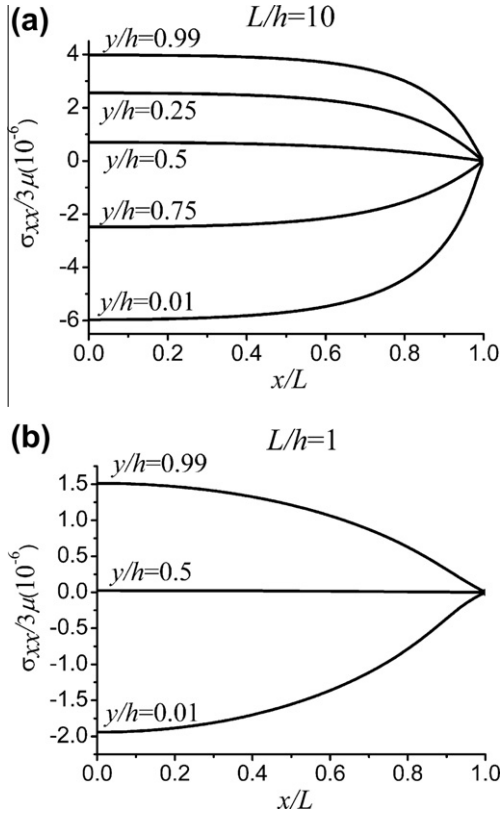

Fig. 11. The distribution of σ_{xx} along the x direction at different height, with $i_0 = 0.75$. (a) $L/h = 10$; (b) $L/h = 1$.

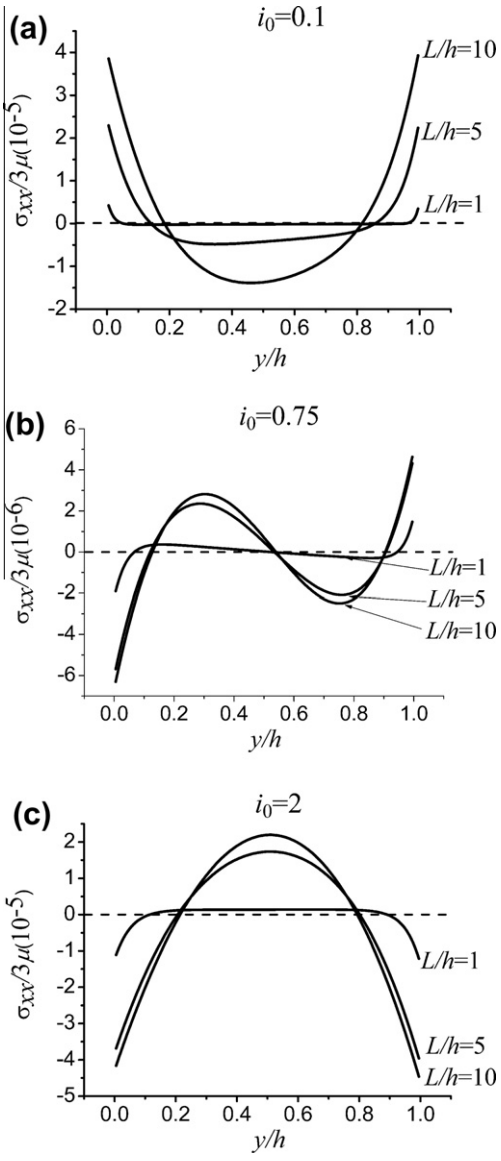

Fig. 12. The distribution of σ_{xx}along the x direction with different $L/h = 10, 5, 1$. (a) $i_0 = 0.1$; (b) $i_0 = 0.75$; (c) $i_0 = 2$.

of the strain distribution should equal the effective curvature k_{eff} obtained from the deflection curve in Fig. 8(a) by using (32). However, Table 1 shows that k_ε is much bigger than k_{eff}. This is again in agreement with the fact observable in Fig. 7 that the transversal cross lines do not remain normal after deformation. Rather, the shear strain is generally not very small as will be shown next. Comparing Fig. 13(a) and (b), we find that $\varepsilon_{yy} = -\nu\varepsilon_{xx}$ is approximately satisfied. Thus, the expansion in height is mainly a Poisson's effect.

4.3. Shears, in plane rotations and quasi-soft behavior

The Cauchy shear stress σ_{xy} was identically zero if the opto-mechanical effect would be homogeneous in the sample as shown

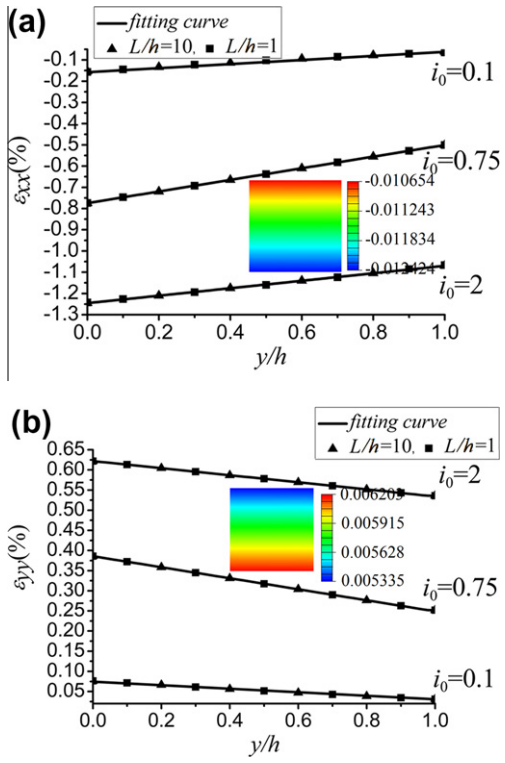

Fig. 13. The distribution of (a) $\varepsilon_{xx}$and (b) ε_{yy} at $x/L = 1/2$ along the height, with $i_0 = 0.1$, 0.75, 2. The contour maps of the strain for $L/h = 1$, $i_0 = 2$ from FEM are attached in the figures.

by the example in Section 3.2 and Fig. 3. This is often expected for soft LCEs that cannot support shear stresses. However, under the linearization assumption and the condition of plane stress problem, we find that σ_{xy} is generally not zero but very small for bended samples under light illuminations, as shown in Fig. 10. This might be due to the fact that the light intensity will decay along the propagation such that the opto-mechanical effect is generally inhomogeneous. Whether the conclusion is true in a general case requires further study.

As shown by the third formula of Eq. (21) in Section 2.3, the Cauchy shear stress σ_{xy} is not only dependent on the Cauchy shear strain ε_{xy} but also the in plane rotation ω_{xy}. They are shown in Fig. 14 together with the effective shear strain ε^g_{xy} for samples under uniform light illuminations.

It is obvious from Fig. 14 that the in plane rotation ω_{xy} is of the same order as the Cauchy shear strain ε_{xy} and both of them are of the same order as the normal strains in Fig. 13. But the effective shear strain ε^g_{xy} is at least one magnitude smaller. This is in consistent with the observation from Fig. 10 that the shear stress σ_{xy} is much smaller than the normal stresses, since it is proportional to ε^g_{xy} by (21), not to ε_{xy}. The distribution of the effective shear strain ε^g_{xy} is also very similar to the shear stress σ_{xy}, and namely ε^g_{xy} is big near the two free corners at the free end and is very small in the middle portion of the slender beam with $L/h = 10$. On the other hand, the distributions of the Cauchy shear strain ε_{xy} and the in plane rotation ω_{xy} shown in Fig. 14 are similar to each other but very different from the shear stress σ_{xy} in Fig. 10. As shown more clearly in Fig. 15, both ε_{xy} and ω_{xy} are approximately linear functions in the length direction but may vary nonlinearly along the height. It seems that the nonlinear variation in y-direction is particularly strong for weak light. This may come from the fact that the decay of the light intensity (2) is closer to the exponential decay thus less linear for weak light as shown by Fig. 5(a).

The above results indicate that the behavior of a LCE specimen under light illuminations is very different from the classical EBBT, namely the shear strain cannot be neglected even for very small deflections of very slender beams. Fig. 16 depicts schematically the light induced bending behavior of LCEs. The middle line of the beam is shown with a bending angle θ_v together with the transversal cross line and the rotated director $\mathbf{n}$.

For infinitesimal deformations considered here, the angle θ_v and the rotation angle of the transversal cross line, θ_c can be calculated as

$$\theta_v = -v_{,x} \quad \text{and} \quad \theta_c = u_{,y} = \theta_v + 2\varepsilon_{xy}. \tag{35}$$

As shown in Fig. 17, they are not equal and seem linear in x direction. According to the approximations of (32) and (34), we can have

$$\theta_v \approx k_{eff}x/h \quad \text{and} \quad \theta_c \approx k_\varepsilon x/h. \tag{36}$$

From Fig. 17, these relations seem to hold and $\theta_c > \theta_v$ in agreement with the fact $k_\varepsilon > k_{eff}$ from Table 1. Thus, the deformed transversal cross line has rotated much more than the middle line such that it does not remain normal any more as indicated in Figs. 7 and 16.

In summary, we have demonstrated that during the light induced bending of beam shaped photochromic LCE samples, the shear stress is generally nonzero but very small; the shear strain is much larger together with rather large in-plane rotation strains. Consequently, the rotation of the transversal cross line after bend-

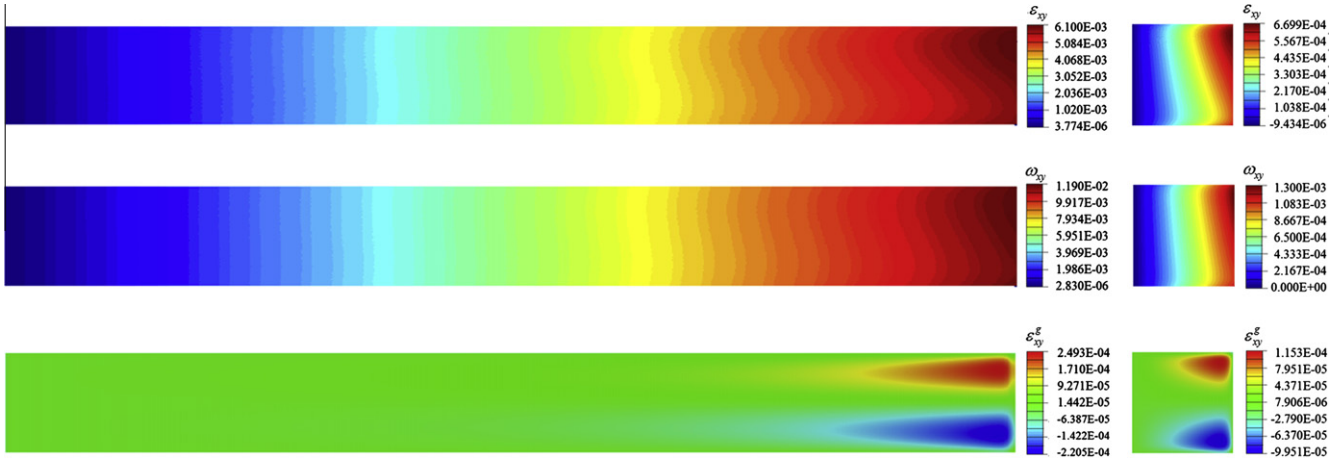

Fig. 14. Contour plots of ε_{xy}, ω_{xy} and ε^g_{xy} of the beam with the initial light intensity $i_0 = 2$.

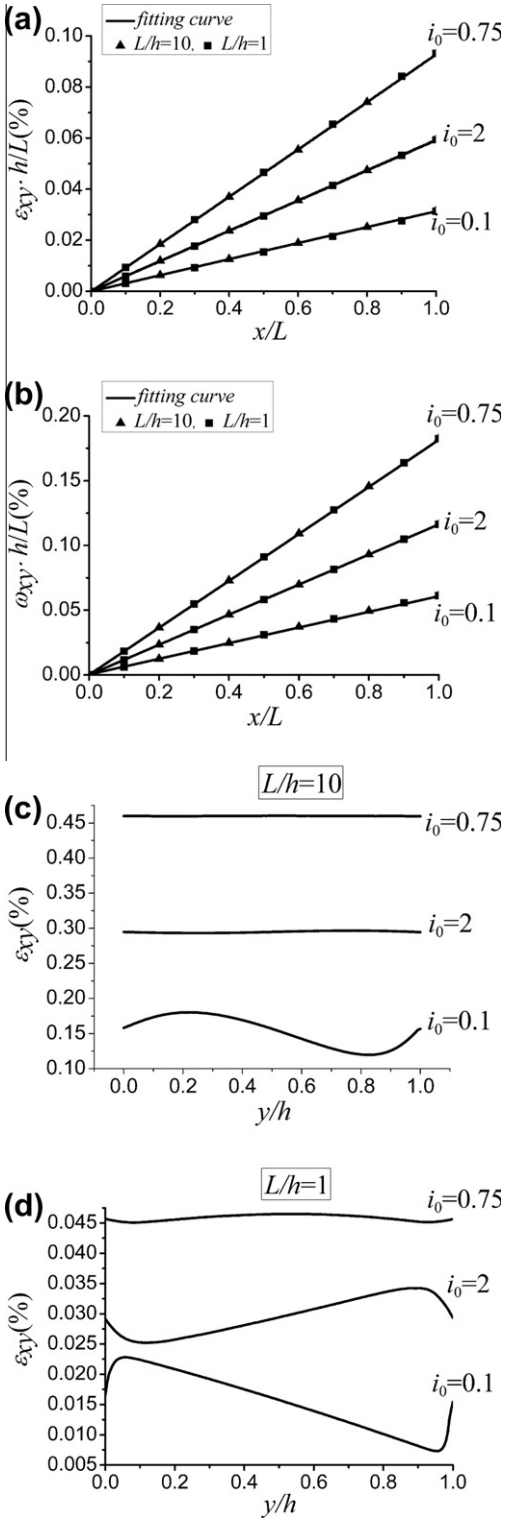

Fig. 15. The variations of (a) ε_{xy} and (b) ω_{xy} along the length. The variation of (c) ε_{xy} for L/h = 10 and (d) ε_{xy} for L/h = 1 along the height, i_0 = 0.1, 0.75, 2.

ing is much stronger than the middle line of the beam, so one of the main assumptions of the classical simple beam theory (EBBT), that the normal cross line remains normal, cannot be applied anymore. Such unusual behavior is certainly resulted from the neo-classical stress–strain relation (5) and (21). The physics underlying the phenomenon is the presence of the liquid crystal phase in the elastomers. In particular, the freedom of rotation of the director field **n**

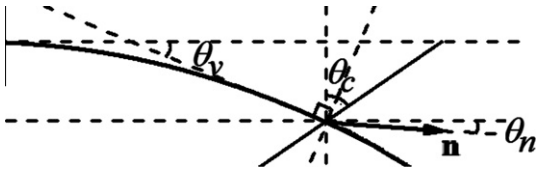

Fig. 16. Schematic representation of the rotations of middle line θ_v, cross line θ_c and director n.

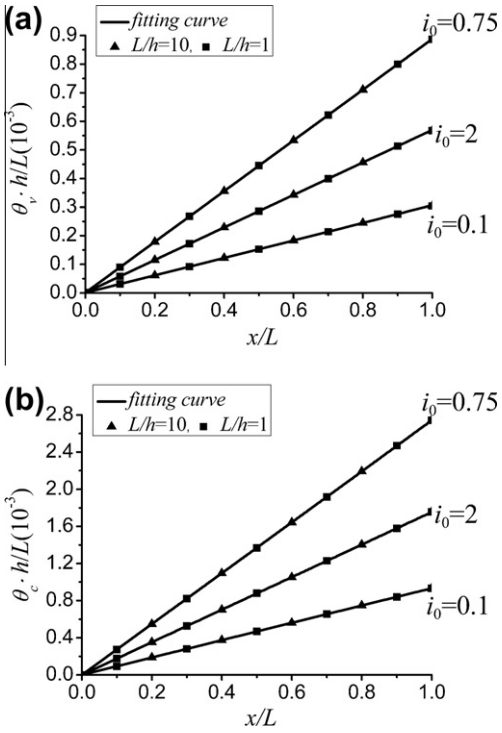

Fig. 17. The variations of the rotation along the length, with i_0 = 0.1, 0.75, 2. (a) the rotation of middle line θ_v; (b) the rotation of cross line θ_c.

is the main reason of soft behaviors in LCEs (DeSimone and Teresi, 2009; Cesana and DeSimone, 2011; Jin et al., 2010b; Warner, 1999;Warner and Terentjev, 2003). Thus, we may call it the quasi-soft opto-mechanical behavior. From Section 2.2, the director is rotated from its original value $\mathrm{n}_0 = (1,0)^T$ to $\mathbf{n} = \mathbf{n}_0 + \delta\ \mathbf{n}$ with an angle θ_n. For the plane stress case, θ_n and $\delta\mathbf{n}$ given by (17) can be obtained as

$$\delta\mathbf{n} = (0, \delta n_y)^T \quad \text{with} \quad \delta n_y = \theta_n = \frac{4r_0^{1/3}}{r_0 - 1}\varepsilon_{xy}^g. \tag{37}$$

Since the effective shear strain is generally much smaller than the Cauchy strains, the rotation of the director should be very small comparing to θ_v and θ_c. As shown in Fig. 18(a), θ_n is at least one magnitude smaller than θ_v along the middle line y = h/2. Its maximum is achieved at the same places as the effective shear strain ε_{xy}^g as shown by Fig. 14, namely near the two corners at the free end. The variation of the director rotation along such maximum path depicts that the magnitude of θ_n is increasing with the length before it reaches the maximum. Then it decays rapidly near $x = L$.

As we know from (20) that the driving force for the director rotation is the shear stress. Since the shear stress is generally very small for the above considered light induced bending of free standing LCE specimens, the director rotation is also very small. However, unlike the usual Hooke's material, small shear stresses do

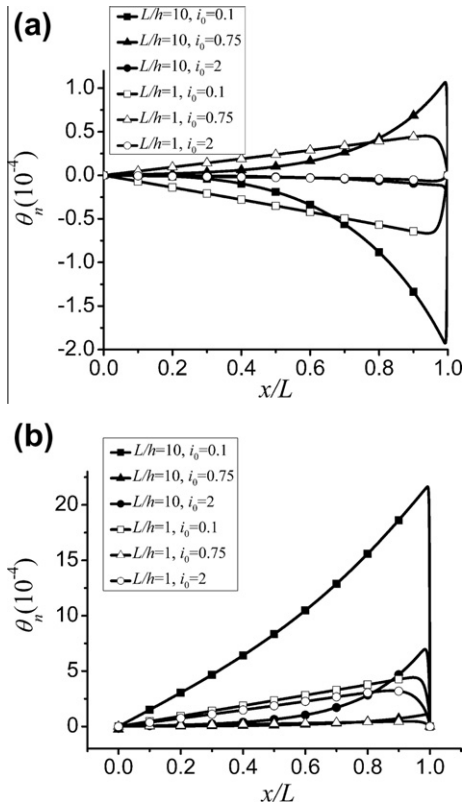

Fig. 18. The variation of θ_n along the length, with $i_0 = 0.1, 0.75, 2$. (a) The path is $y = h/2$; (b) The path is that θ_n reaches the maximum in the whole beam.

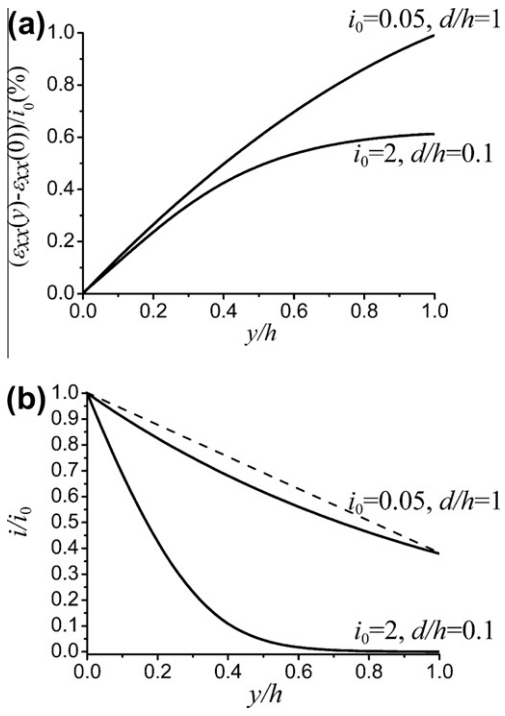

Fig. 19. (a) The variation of scaled normal strain along the height. (b) The variation of intensity along the height, with $i_0 = 0.05$, $d/h = 1$ and $i_0 = 2$, $d/h = 0.1$.

not necessarily imply small shear strains for LCEs. The unusual constitutive behavior given by the third formula of Eq. (21) is responsible for the above quasi-soft opto-mechanical behavior. And even for very slender specimen and very small bending magnitude, the classical EBBT is not applicable for light induced bending of LCE materials. Rather, the effect of the shear strain must be considered. This is rather surprising at the first glance and is in contraction to most of the existing analysis of the light induced bending of LCEs in the literatures (Corbett and Warner, 2007, Corbett and Warner, 2008; Dunn, 2007; Dunn and Maute, 2009; Jin et al., 2010a; Modes et al., 2010;Warner and Mahadevan, 2004; Warner et al., 2010a; Warner et al., 2010b; Warner et al., 2011). More works should be done to modify the classical EBBT to include such shear effects.

4.4. Two examples with non-planar deformed cross section

In all the above numerical simulations, the transversal cross lines remain approximately straight after the light induced bending as indicated by the linearity of the normal strain ε_{xx} as shown in Fig. 13(a) given by Eq. (34). However, this is not always the case even for very slender beam shaped specimen due to the special opto-mechanical coupling in this material. Due to the length limitation, we shall give just two examples here and leave the detailed analysis to a forthcoming paper. Only slender beam shaped specimen $L/h = 10$ will be considered here.

As shown in Fig. 19(a), the specimen is under uniform light illumination from the bottom. The normal strain ε_{xx} are far from linear for very weak light intensity $i_0 = 0.05$ with $d/h = 1$ and for very short decay distance $d/h = 0.1$ with $i_0 = 2$. This is resulted from the nonlinear light absorption given by (2), since the light intensities are quite far from linear inside the specimen for these two cases as shown in Fig. 19(b).

5. Conclusions

In this paper, the light-induced constitutive relations are obtained by introducing the photoisomerization and its effect on the nematic-isotropic transitions into the nonlinear constitutive equations of LCEs which are based on the neo-classical elastic free energy. We linearize the stress–strain relation based on the assumption of infinitesimal strains and ignore the effect of the deformation on the light propagation and the effect of the stress on the order parameters. The result shows that the Cauchy stress tensor is a function of both the symmetric part of the displacement gradient $\boldsymbol{\varepsilon}$ and the asymmetric part $\boldsymbol{\omega}$. The shear stress in the plane perpendicular to the director is not zero but proportional to the rotation of the director.

Plane stress problems are considered for simplicity. The reduced normal stress–strain relations have similar expressions as the linear thermal elastic materials with the thermal strain replaced by an anisotropic opto strain which is a contraction along the LC director and an expansion in the perpendicular direction. However, the shear stress is not proportional to the Cauchy shear strain any more but also depends on the in-plane rotation (the asymmetric part of displacement gradient).

Although, the obtained constitutive relation is very unusual, it is possible for us to rescale the displacements and use commercial FEA software ABAQUS to carry out the numerical simulations of light induced bending of two dimensional specimens. Of course, secondary development with self-defined material subroutines is inevitable.

The numerical results have shown that the light induced contraction and bending of two dimensional specimens can be simulated by our model. It is found that if the decay distance of the light due to the absorption is much large than the height of the specimen, approximately homogeneous contraction in length and expansion in height can be induced by uniform light illuminations. If the ratio of decay distance vs. height, d/h is not too large, the specimen will bend toward the incoming light in addition to a

contraction in length and expansion in height. The bending seems quite identical for long and short specimens but depend strongly on the incoming light intensity. The dependence of the bending magnitude on the light intensity is generally non-monotonic, increasing firstly to a maximum and then decreasing to zero for very large light.

The distributions of the stresses and strains are analyzed in some details for specimens under uniform light illuminations. The results indicate that the driving force for the light induced bending is the normal stress component in the direction of the LC director. The other stress components are generally much smaller even for very short specimen. The distribution of the main stress component along the height is highly nonlinear and depends strongly on the light intensity, which is very similar to the results obtained by using elementary beam theory (Jin et al., 2010a).

Although the shear stress is very small comparing to the main stress component, it is generally not zero under light illuminations in contrast to pure mechanical loading of soft LCEs. Moreover, the Cauchy shear stain is generally not small but in the same order as the other normal strain components. Thus, the deformed transversal cross line does not remain normal any more, although it can remain straight after the light induced bending if the light intensity or the decay distance is not too small and the LCE specimen is in the deep nematic phase. Therefore, the classical Euler–Bernoulli Beam Theory cannot be directly applied to model the light induced bending of soft LCEs. Some shear effect must be considered.

The above unusual quasi-soft opto-mechanical behavior is certainly a consequence of the constitutive relations based on the neoclassical elastic energy of LCEs. However, it is known that the real behavior of LCE materials cannot be properly described by this free energy alone. In particularly, the rotation of the LC director should not be completely free in cross-linked solid materials. Thus, it is worthwhile to carry out further calculations by using some modified constitutive equations such as the semi-soft elastic energy (Cesana and DeSimone, 2011), phase field model (Oates and Wang, 2009), dynamical model (Zhu et al., 2011) etc.

Acknowledgments

Lin and Huo thank the support of the National Natural Science Foundation of China (No. 11072062 & 11172068) and the Research Fund for the Doctoral Program of Higher Education of China (20110071110013).

References

Agostiniani, V., DeSimone, A., 2011. Γ-convergence of energies for nematic elastomers in the small strain limit. Contin. Mech. Thermodynam. 23, 257–274.
Camacho-Lopez, M., Finkelmann, H., Palffy-Muhoray, P., 2004. Fast liquid crystal elastomer swims into the dark. Nat. Mater. 3, 307–310.
Cesana, P., DeSimone, A., 2011. Quasiconvex envelopes of energies for nematic elastomers in the small strain regime and applications. J. Mech. Phys. Solids 59, 787–803.
Chen, H., He, L., 2008. Photoinduced surface topography of nematic elastomers: a Green function approach. J. Phys. Condens. Mater. 20, 285107.
Conti, S., DeSimone, A., Dolzmann, G., 2002a. Soft elastic response of stretched sheets of nematic elastomers: a numerical study. J. Mech. Phys. Solids 50, 1431–1435.
Conti, S., DeSimone, A., Dolzmann, G., 2002b. Semi-soft elasticity and director reorientation in stretched sheets of nematic elastomers. Phys. Rev. E 60, 61710.
Corbett, D., Warner, M., 2007. Linear and nonlinear photoinduced deformations of cantilevers. Phys. Rev. Lett. 99, 174302.
Corbett, D., Warner, M., 2008. Bleaching and stimulated recovery of dyes and of photocantilevers. Phys. Rev. E 77, 051710.
Cviklinski, J., Tajbakhsh, A.R., Terentjev, E.M., 2002. UV isomerization in nematic elastomers as a route to photo-mechanical transducer. Eur. Phys. J. E9, 427–434.
Dawson, N.J., kuzyk, M.G., Neal, J., Luchette, P., palffy-Muhoray, P., 2011. Experimental studies of the mechanisms of the photomechanical effects in a nematic liquid crystal elatomer. J. Opt. Soc. Amer. A: 28, 1916–1921.
de Gennes, P.G., 1982. In Polymer Liquid Crystals. Academic Press, New York.
de Gennes, P.G., Prost, J.P., 1994. The Physics of Liquid Crystals. Oxford University Press, Oxford.
DeSimone, A., Teresi, L., 2009. Elastic energies for nematic elastomers. Eur. Phys. J. E 29, 191–204.
Dunn, M.L., 2007. Photomechanics of mono- and polydomain liquid crystal elastomer films. J. Appl. Phys. 102, 013506.
Dunn, M.L., Maute, K., 2009. Photomechanics of blanket and patterned liquid crystal elastomer films. Mech. Mater. 41, 1083–1089.
Finkelmann, H., Nishikawa, E., Pereira, G.G., Warner, M., 2001. A new opto-mechanical effect in solids. Phys. Rev. Lett. 87, 015501.
He, L., 2007. Surface deformation of nematic elastomers under striped illumination. Phys. Rev. E 75, 041702.
Hogan, P.M., Tajbakhsh, A.R., Terentjev, E.M., 2002. UV manipulation of order and macroscopic shape in nematic elastomers. Phys. Rev. E 65, 041720.
Ikeda, T., 2003. Photomodulation of liquid crystal orientations for photonic applications. J. Mater. Chem., 13.
Jiang, X., Zhang, T., Ding, S., Huo, Y., 2010. Effect of self-heating on photo-mechanical behavior of nematic elastomers. Thermochim. Acta 500, 44–50.
Jin, L., Jiang, X., Huo, Y., 2006. Light-induced nonhomogeneity and gradient bending in photochromic liquid crystal elastomers. Sci. China Ser. G—Phys. Mech. Astron. 49, 553–563.
Jin, L., Yan, Y., Huo, Y., 2010a. A gradient model of light-induced bending in photochromic liquid crystal elastomer and its nonlinear behaviors. Int. J. Non Linear Mech., 45.
Jin, L., Zeng, Z., Huo, Y., 2010b. Thermomechanical modeling of the thermo-order-mechanical coupling behaviors in liquid crystal elastomers. J. Mech. Phys. Solids 58 (11), 1907–1927.
Jin, L., Lin, Y., Huo, Y., 2011. A large deflection light-induced bending model for liquid crystal elastomers under uniform or nonuniform illumination. Int. J. Solids Struct. 48, 3232–3242.
Modes, C.D., Bhattacharya, K., Warner, M., 2010. Gaussian curvature from flat elastica sheets. Proc. Roy. Soc. A: Math. Phys. Eng. Sci. 467, 1121–1140.
Olmsted, P., 1994. Rotational invariance and Goldstone modes in nematic elastomers and gels. J. Phys. II France 4, 2215–2230.
Oates, W.S., Wang, H., 2009. A new approach to modeling liquid crystal elastomers using phase field methods. Model. Simul. Mater. Sci. Eng. 17, 064004.
Saleh, B.E.A., Teich, M.C., 1991. Fundamentals of Photonics. John Wiley & Sons, New York.
Verwey, G.C., Warner, M., 1995. Soft rubber elasticity. Macromolecules 28, 4303–4306.
van Oosten, C.L., Harris, K.D., Bastiaansen, C.W., Broer, D.J., 2007. Glassy photomechanical liquid-crystal network actuators for microscale devices. Eur. Phys. J. E 23, 329–336.
Warner, M., Bladon, P., Terentjev, E.M., 1994. Soft elasticity-deformation without resistance in liquid-crystal elastomers. J. Phys. II France 4, 93–102.
Warner, M., 1999. New elastic behaviour arising from the unusua constitutive relation of nematic solids. J. Mech. Phys. Solids, 1355–1377.
Warner, M., Terentjev, E.M., 2003. Liquid Crystal Elastomers. Clarendon Press, Oxford.
Warner, M., Mahadevan, L., 2004. Photoinduced deformations of beams, plates, and films. Phys. Rev. Lett. 92, 21–25.
Warner, M., Modes, C.D., Corbett, D., 2010a. Curvature in nematic elastica responding to light and heat. Proc. R. Soc. A 466, 2975–2989.
Warner, M., Modes, C.D., Corbett, D., 2010b. Suppression of curvature in nematic elastica. Proc. R. Soc. A 466, 3561–3578.
Warner, M., Modes, C.D., Corbett, D., 2011. Curvature and its suppression in nematic elastica responding to light and heat. Proc. R. Soc. A 466, 2975–2989.
Yu, Y., Nakano, M., Ikeda, T., 2003. Directed bending of a polymer film by light. Nature 425, 145.
Zeng, Z., Jin, L., Huo, Y., 2010. Strongly anisotropic elastic moduli of nematic elastomers: analytical expressions and nonlinear temperature dependence. Eur. Phys. J. E 32 (1).
Zhu, W., Shelley, M., Palffy-Muhoray, P., 2011. Modeling and simulation of liquid-crystal elastomers. Phys. Rev. E 83, 051703.